CrossMark

ORIGINAL PAPER

Highly improved sensing of dopamine by using glassy carbon electrode modified with MnO$_2$, graphene oxide, carbon nanotubes and gold nanoparticles

Dejiang Rao[1] · Xinjin Zhang[1] · Qinglin Sheng[1] · Jianbin Zheng[1]

Abstract A composite material obtained by ultrasonication of graphene oxide (GO) and multi-walled carbon nanotubes (MWCNTs) was loaded with manganese dioxide (MnO$_2$), poly(diallyldimethylammonium chloride) and gold nanoparticles (AuNPs), and the resulting multilayer hybrid films were deposited on a glassy carbon electrode (GCE). The microstructure, composition and electrochemical behavior of the composite and the modified GCE were characterized by transmission electron microscopy, Raman spectra, energy-dispersive X-ray spectroscopy, electrochemical impedance spectroscopy and cyclic voltammetry. The electrode induces efficient electrocatalytic oxidation of dopamine at a rather low working voltage of 0.22 V (vs. SCE) at neutral pH values. The response is linear in the 0.5 μM to 2.5 mM concentration range, the sensitivity is 233.4 μA·mM^{-1}·cm^{-2}, and the detection limit is 0.17 μM at an SNR of 3. The sensor is well reproducible and stable. It displays high selectivity over ascorbic acid, uric acid and glucose even if these are present in comparable concentrations.

✉ Qinglin Sheng
qinglinsheng@126.com

✉ Jianbin Zheng
zhengjb@nwu.edu.cn

[1] Institute of Analytical Science, Shaanxi Provincial Key Laboratory of Electroanalytical Chemistry, Northwest University, Xi'an, Shaanxi 710069, China

Introduction

Dopamine (DA), a neurotransmitter, plays a significant role in neuroregulation, cardiovascular and circulatory systems [1, 2]. The level of DA in the human body is closely related to many mental illnesses [3]. Therefore, selective and sensitive detection of DA is of great meaning. So far, many reported methods have been applied to the detection of DA, such as mass spectrometry, fluorescence spectrometry and electrochemical method [4–6]. Among these methods, electrochemical method is widely used for detection of DA because DA is easy to be oxidized electrochemically [7]. In particular, the non-enzymatic electrochemical sensor has been extensively adopted for the detection of DA because of their advantages of simplicity, sensitivity and cost-effectiveness [8, 9].

Graphene oxide (GO) has potential applications in the construction of non-enzymatic electrochemical sensors due to its advantages of good dispersion and variety of functionalization methods [10, 11]. Meanwhile, multi-walled carbon nanotubes (MWCNTs) have been widely used in the construction of non-enzymatic electrochemical sensors due to their high surface area to volume ratio and chemical stability [12, 13]. GO-MWCNT composites are beneficial to enhance the electron transfer efficiency because the introduction of MWCNTs contributes to increase the specific surface area of GO sheets [13, 14]. Consequently, the GO-MWCNT composites have been well developed in the study of electrochemical sensing [15, 16].

Manganese dioxide (MnO$_2$) has been used in the electrochemical detection of hydrogen peroxide and cysteine, attributing to its advantages of excellent electrochemical properties, cheapness and simple synthesis [17, 18]. Therefore, MnO$_2$ can be used as a catalyst for the electrochemical detection of DA [19]. In recent years, noble metal nanoparticles were proved to be able to enhance the performance of non-enzymatic sensors [20]. Particularly, gold nanoparticles

🙋 Springer

(AuNPs) have been introduced into the study of electrochemical sensors due to their good conductivity, excellent electrocatalytic activity and biocompatibility [21, 22]. Poly(diallyldimethylammonium chloride) (PDDA) was easily modified and stabilized AuNPs in aqueous solution [23]. Thus, the negatively charged AuNPs can be self-assembled onto the films of negatively charged MnO_2 decorated GO-MWCNT composites with PDDA as a coupling agent.

Herein, GO-MWCNT/MnO_2/AuNP nanocomposites were successfully synthesized by using PDDA as a coupling agent. Further, a non-enzymatic electrochemical sensor of DA based on a glassy carbon electrode (GCE) modified with the GO-MWCNT/MnO_2/AuNP nanocomposites was designed. The obtained results indicated that this DA sensor can be used to detect a real sample.

Experimental

Materials and reagents

Graphite powder (99.998 %, 325 mesh) was purchased from Shanghai Yuanju Biotechnology Co., Ltd. (Shanghai, China, http://www.yjbiotech.cn/); ethylene glycol and sodium citrate were got from Tianjin Tianli Chemistry Reagent Co., Ltd. (Tianjin, China, http://www.tianli-tj.com/ht_world/chanpin1/index.asp); uric acid (UA), ascorbic acid (AA), DA, PDDA (Mw: 40,000–50,000) and MWCNTs (purity >95 wt%) were provided by Aladdin Industrial Corporation (Shanghai, China, http://www.aladdin-e.com/); $HAuCl_4 \cdot 4H_2O$ (purity >99.9 %) was obtained from Shanghai Reagent Factory (Shanghai, China, http://shiyicr.company.lookchem.cn/). The 0.1 $mol \cdot L^{-1}$ phosphate buffer saline (PBS, pH 7.0) was used as electrolyte in electrochemical studies. The other reagents and chemicals used were of analytical reagent grade. The deionized water was prepared by a Millipore device (Milli-Q, China, resistivity >18 $M\Omega \cdot cm$, http://www.merckmillipore.com/CN/zh?bd=1).

Apparatus and electrochemical measurements

The morphology of the obtained samples was characterized by transmission electron microscopy (TEM) using a Tecnai G^2 F20 S-TWIN (FEI, USA) measurement. The composition of GO-MWCNT/MnO_2/AuNP nanocomposites was identified by energy-dispersive X-ray spectroscopy (EDS) using a JSM-6700F (JEOL, Japan) measurement. The Raman spectrograms were obtained by using a Raman spectrometer (LABRAM-HR, France) with an excitation wavelength of 632.8 nm. The study of electrochemical behavior was performed on a CHI 660D electrochemical workstation (Shanghai CH Instrument Co., Ltd., China, http://www.chinstr.com/) with a three-electrode cell. Here, a bare GCE

(diameter: 3.0 mm), GO-MWCNT composites modified GCE (GO-MWCNT/GCE), GO-MWCNT/MnO_2 composites modified GCE (GO-MWCNT/MnO_2/GCE) and GO-MWCNT/MnO_2/AuNP nanocomposites modified GCE (GO-MWCNT/MnO_2/AuNP/GCE) were adopted as working electrodes, respectively. Saturated calomel electrode (SCE) and platinum wire electrode were used as reference electrode and counter electrode, respectively. This study was conducted at the room temperature 25 ± 2 °C.
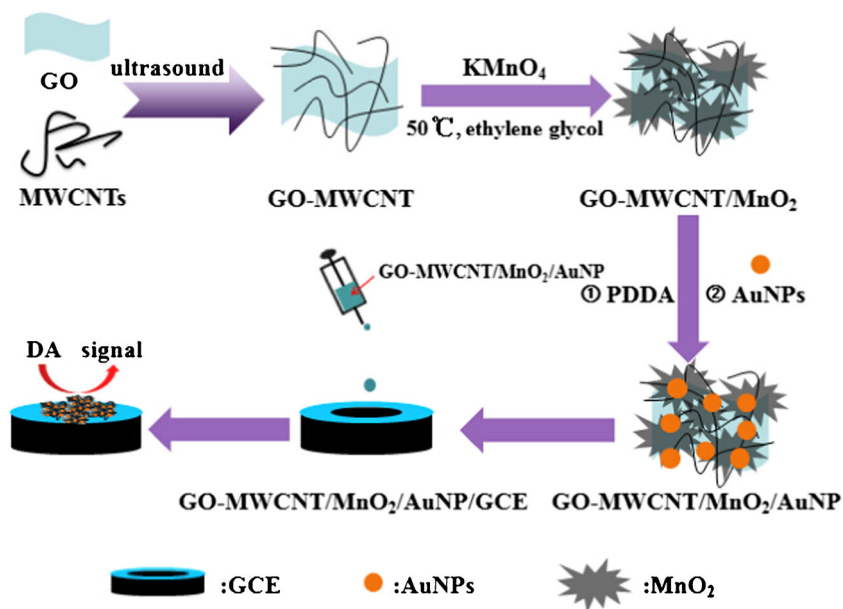
Fabrication of the sensor

Synthesis of GO-MWCNT and GO-MWCNT/MnO_2 composites

The GO was prepared by an improved Hummers' approach [24]. GO-MWCNT composites were prepared by the previous method with minor changes [16]. The detailed preparation process of GO-MWCNT composites was given in the Electronic Supporting Material (ESM). The GO-MWCNT/MnO_2 composites were prepared by ethylene glycol reduction method. Briefly, the obtained GO-MWCNT composites powder (20.0 mg) was thoroughly dispersed in 24.0 mL of deionized water through continuous ultrasound. After that, 43.6 mg $KMnO_4$ was added to the GO-MWCNT suspension and kept stirring for 30 min. Next, ethylene glycol was subsequently added to the above mixture solution in a water bath of 50 °C until the purple red of the $KMnO_4$ was faded. The black products were collected by centrifugation at the speed of 5000 rpm and the relative centrifugation force of 2776 g for 3 min, washed twice with deionized water and then dried in an oven at 50 °C for 8 h.

Synthesis of GO-MWCNT/MnO_2/AuNP nanocomposites

The schematic illustration of the preparation of GO-MWCNT/MnO_2/AuNP nanocomposites is illustrated in Scheme 1. Herein, the GO-MWCNT/MnO_2/AuNP nanocomposites were obtained by a self-assembled method using PDDA as a coupling agent. Firstly, the AuNPs suspension was synthesized by the reported approach [25]. The detailed experimental data is given in the ESM. The PDDA functionalized GO-MWCNT/MnO_2 was obtained according to the previous methods with minor modifications [23]. Briefly, 10.0 mg of GO-MWCNT/MnO_2 powder was completely dispersed in 20.0 mL of deionized water containing 0.2 % PDDA and 0.5 $mol \cdot L^{-1}$ NaCl. The mixture solution was ultrasonicated for 1.5 h. After that, the PDDA functionalized GO-MWCNT/MnO_2 were collected by centrifugation at the speed of 5000 rpm and the relative centrifugation force of 2776 g for 5 min. At last, the 3.0 mL AuNPs suspension was added to 3.0 mL PDDA functionalized GO-MWCNT/MnO_2 suspension (1.0 $mg \cdot mL^{-1}$) and kept stirring for 30 min. These expected products were obtained by

Modification of electrode

The GCE was polished using alumina powder (1.0 μm followed by 0.3 μm) to obtain a mirror-like surface. After that, GCE was ultrasonically washed in ethanol-water (1:1, v/v ratio) solution and deionized water for 3 min, respectively. The schematic illustration of the preparation GO-MWCNT/MnO$_2$/AuNP/GCE is also shown in Scheme 1. The common drop-coating method was used to modify the polished GCE. Briefly, GO-MWCNT/MnO$_2$/AuNP powder (1.0 mg) was completely dispersed in deionized water (1.0 mL). After that, the obtained dispersion (5.0 μL, 1.0 mg·mL^{-1}) was dropped to the mirror-like surface of GCE and dried in air at room temperature.

## Results and discussion

Optimization of the method

The following parameters were optimized: (a) pH value of the supporting electrolyte; (b) volume of the AuNPs suspension (V_{AuNPs}); (c) applied potential of the amperometric response. Respective data and Figures are given in the ESM. The following experimental conditions were found to give best results: (a) the supporting electrolyte pH value of 7.0; (b) the V_{AuNPs} of 3.0 mL; (c) the applied potential of 0.2 V.

centrifugation at the speed of 5000 rpm and the relative centrifugation force of 2776 g for 4 min, washed three times with deionized water and dried in an oven at 50 °C for 8 h.

Characterization of GO-MWCNT/MnO$_2$/AuNP nanocomposites

Figure 1 shows the TEM images of GO (A), GO-MWCNT composites (B), AuNPs (C), GO-MWCNT/MnO$_2$ composites (D, E, F) and GO-MWCNT/MnO$_2$/AuNP nanocomposites (G, H, I). The smooth surface of GO with some wrinkles was observed in Fig. 1A. As shown in Fig. 1B, MWCNTs with different orientations and lengths were successfully modified onto the surface of GO sheets. Figure 1C indicates that AuNPs have a nanoscale spherical shape with a diameter of 10 ± 2 nm. As shown in Fig. 1D and E, the uniform layered MnO$_2$ were wrapped on the surface of GO-MWCNT composites. The multilayer structure is composed of GO sheets, MWCNTs and layered MnO$_2$, as proved in Fig. 1D and F. As illustrated in Fig. 1G and H, the AuNPs uniformly deposited on the surface of GO-MWCNT/MnO$_2$ composites and no aggregation was observed. Moreover, the well-dispersed AuNPs, layered MnO$_2$, MWCNTs and GO with some wrinkles were clearly observed. Figure 1I indicates that AuNPs were well dispersed on the surface of multilayer film composing of GO, MWCNTs and MnO$_2$, suggesting that the GO-MWCNT/MnO$_2$/AuNP nanocomposites were successfully synthesized by the self-assembled method. The composition of GO-MWCNT/MnO$_2$/AuNP nanocomposites was identified by EDS. As illustrated in Fig. 1J, the GO-MWCNT/MnO$_2$/AuNP nanocomposites are composed of C, N, O, Mn, Cl and Au elements. Additionally, peaks at the region of 3–4 KeV were assigned to the signals of conductive glass coated with indium tin oxide (ITO) [13]. Fig. S1 (ESM) shows the Raman spectrograms of (a) GO, (b) GO-MWCNT composites and (c) GO-MWCNT/MnO$_2$/

Fig. 1 TEM images of GO (**a**), GO-MWCNT composites (**b**), AuNPs (**c**, GO-MWCNT/MnO₂ composites (**d**, **e**, **f**) and GO-MWCNT/MnO₂/AuNP nanocomposites (G, H, I); EDS spectrum of GO-MWCNT/MnO₂/AuNP nanocomposites on ITO (J)
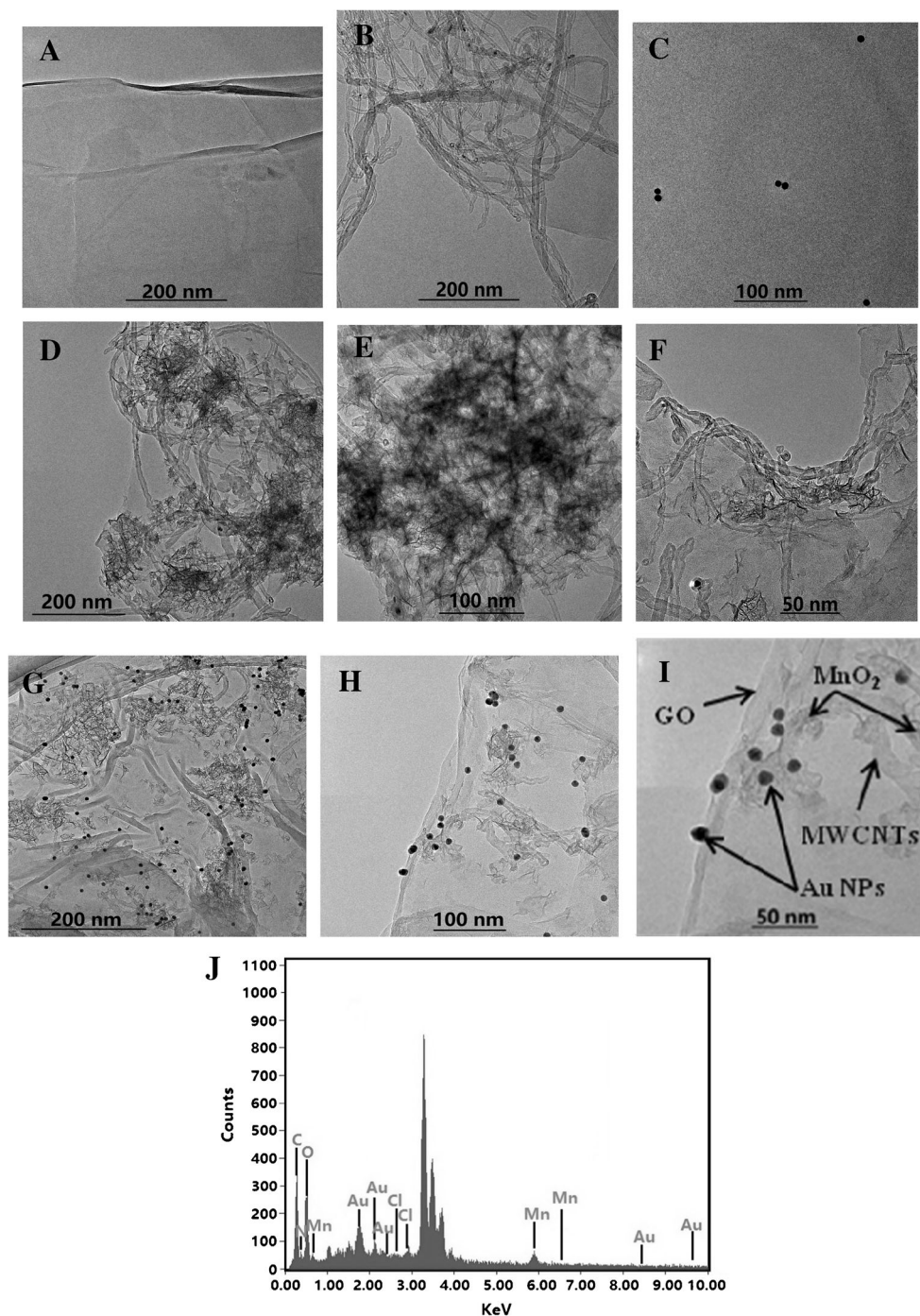
AuNP nanocomposites. It can be observed that there are two broad peaks of the Raman spectrogram of (a) GO at 1330 and 1590 cm⁻¹, corresponding to the D and G bands, respectively [26]. The peak intensity ratio of the D and G band (I_D/I_G) is about 1.2 for GO samples. As expected, the spectrogram of GO is in good agreement with the reported literature [14]. According to the Raman spectrograms of (a) GO and (c) GO-MWCNT/MnO₂/AuNP nanocomposites, the I_D/I_G has not changed dramatically, indicating that the reduction of GO did not occur. As shown in Fig. S1

(ESM), compared with the Raman spectrogram of GO, the red shift of GO-MWCNT composites (b) was clearly observed [26]. Moreover, the intensity of the Raman spectrogram of GO-MWCNT/MnO₂/AuNP nanocomposites is enhanced somewhat compared to that of GO samples, suggesting a consistency with the reported literature [27]. On the basis of characterization of TEM, Raman spectra and EDS, it can be strongly proved that the GO-MWCNT/MnO₂/AuNP nanocomposites were successfully synthesized by this synthetic method.

Electrochemical behavior of GO-MWCNT/MnO$_2$/AuNP nanocomposites

The surface characteristics of modified electrodes were investigated by electrochemical impedance spectroscopy (EIS). The semicircle's diameter of Nyquist plot is equal to the electron transfer resistance (R_{et}) [28]. As shown in Fig. 2A, the GCE has a quite small R_{et} value. The R_{et} values for different working electrodes were calculated in the following sequence: GO-MWCNT/GCE (185.0 ± 2.3 Ω, n = 3) > GO-MWCNT/MnO$_2$/GCE (96.0 ± 1.8 Ω, n = 3) > GO-MWCNT/MnO$_2$/AuNP/GCE (40.0 ± 2.6 Ω, n = 3) > GCE (28.0 ± 1.6 Ω, n = 3). In contrast, the values of R_{et} for GO-MWCNT/MnO$_2$/GCE decreased to 40.8 ± 0.8 Ω after the well-dispersed AuNPs were uniformly deposited onto the surface of GO-MWCNT/MnO$_2$ composites, suggesting that the GO-MWCNT/MnO$_2$/AuNP nanocomposites can enhance the electron transfer rate. The cyclic voltammograms (CVs) of different working electrodes in 0.10 mol L^{-1} PBS (pH 7.0) in the absence (curve a, c, e and g) and presence (curve b, d, f and h) of 0.5 mM DA at a scan rate of 0.1 V·s^{-1} were shown in Fig. 2B and C. The red arrow indicates the direction of sweep. As shown in Fig. 2B, the well-defined redox process (curve b) for bare GCE in 0.10 mol L^{-1} PBS (pH 7.0) in the presence of 0.5 mM DA was observed. All working electrodes have no obvious oxidation peak current (I_{pa}) and reduction peak current (I_{pc}) response in the absence of DA. After the addition of 0.5 mM DA, the I_{pa} and I_{pc} of DA at different modified

electrodes (curve d, f, h) increased by different degrees. The I_{pa} of DA on the GO-MWCNT/MnO$_2$/AuNP/GCE was located at about 0.16 V. Moreover, compared with GO-MWCNT/MnO$_2$/GCE, the I_{pa} of DA at the GO-MWCNT/MnO$_2$/AuNP/GCE showed an increase of 141.4 % from 11.1 ± 0.11 to 26.8 ± 0.21 μA, indicating that the GO-MWCNT/MnO$_2$/AuNP nanocomposites exhibited excellent electrocatalytic properties towards the oxidation of DA. The oxidation of DA on the GO-MWCNT/MnO$_2$/AuNP/GCE was attributed to the synergistic catalysis among GO-MWCNT composites, MnO$_2$ and AuNPs. According to the previous literatures, the possible electrooxidation mechanism of DA on the GO-MWCNT/MnO$_2$/AuNP/GCE was acquired [6, 29]. The electrooxidation of DA on the GO-MWCNT/MnO$_2$/AuNP/GCE involves two electrons transferred process. The net reaction of mechanism is given in Fig. S3 (ESM).

Figure 3A shows the electrocatalytic ability of GO-MWCNT/MnO$_2$/AuNP/GCE towards the oxidation of DA by changing its concentrations. When DA was introduced into 0.1 mol·L^{-1} PBS (pH 7.0), the I_{pa} and I_{pc} appeared and progressively increased, suggesting a remarkable electrocatalytic ability for DA. Moreover, as shown in Fig. 3A (inset), I_{pa} and I_{pc} of DA between its concentrations from 0.1 to 0.9 mM show good linear relationship with a correlation coefficient (r) of 0.9990 and 0.9989, respectively. These results indicated that GO-MWCNT/MnO$_2$/AuNP can be potentially applied to quantitatively detect DA. Figure 3B shows the CVs of GO-MWCNT/MnO$_2$/AuNP/GCE in 0.1 mol·L^{-1} PBS (pH 7.0)

Fig. 2 **a** Nyquist plots of (a) the bare GCE, (b) GO-MWCNT/GCE, (c) GO-MWCNT/MnO$_2$/GCE and (d) GO-MWCNT/MnO$_2$/AuNP/GCE in 0.10 mol L^{-1} PBS (pH 7.0) containing 5.0 mM [Fe(CN)$_6$]$^{4-/3-}$ at open-circuit potential conditions (AC amplitude: 5.0 mV); **(b)** and **(c)** CVs obtained by (a, b) the bare GCE, (c, d) GO-MWCNT/GCE, (e, f) GO-MWCNT/MnO$_2$/GCE and (g, h) GO-MWCNT/MnO$_2$/AuNP/GCE in 0.10 mol L^{-1} PBS (pH 7.0) in the absence (a, c, e and g) and presence (b, d, f and h) of 0.5 mM DA at a scan rate of 0.1 V·s^{-1}
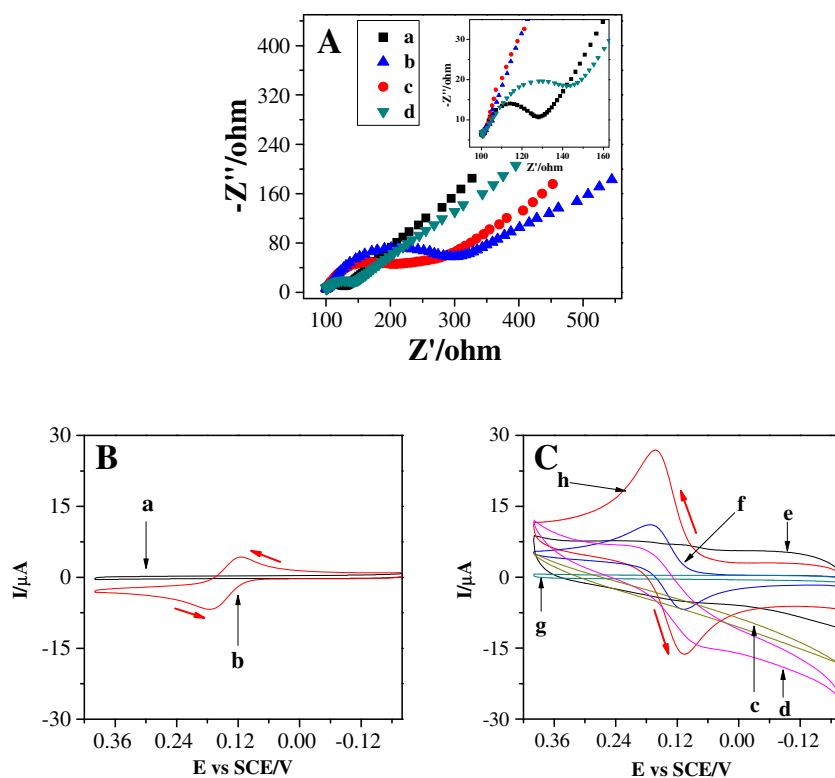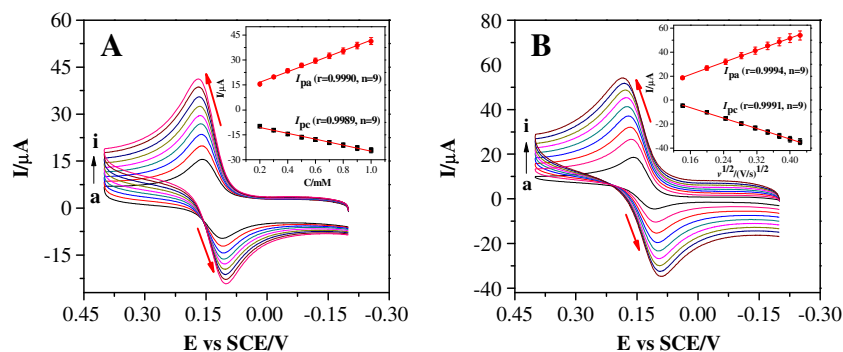
Fig. 3 a CVs obtained by GO-MWCNT/MnO$_2$/AuNP/GCE in the presence of different DA concentrations (From a to i: 0.1, 0.2, 0.3, 0.4, 0.5, 0.6, 0.7, 0.8 and 0.9 mM) in 0.1 mol·L^{-1} PBS (pH 7.0) at a scan rate of 0.1 V s^{-1}; **Inset:** linear fitting chart of I_{pa} and I_{pc} of DA versus its concentrations (C/mM). **b** CVs obtained by GO-MWCNT/MnO$_2$/ AuNP/GCE in 0.1 mol·L^{-1} PBS (pH 7.0) containing 1.0 mM DA with different scan rates (From a to i: 0.02, 0.04, 0.06, 0.08, 0.10, 0.12, 0.14, 0.16 and 0.18 V s^{-1}); **Inset:** linear fitting chart of I_{pa} and I_{pc} of DA versus $v^{1/2}$

containing 1.0 mM DA with different scan rates (v). As proved in Fig. 3B, the I_{pa} and I_{pc} of DA increased with increasing of scan rates from 0.02 to 0.18 V s^{-1}. As shown in Fig. 3B (inset), the I_{pa} and I_{pc} of DA gradually increased in a good linear relationship ($r = 0.9994$ and 0.9991, respectively) with the square root of scan rates ($v^{1/2}$) in the range of 0.02– 0.18 V s^{-1}. These results strongly demonstrated that this electrocatalytic process on GO-MWCNT/MnO$_2$/AuNP/GCE was diffusion-controlled.

Figure 4A shows the amperometric response of DA at the GO-MWCNT/MnO$_2$/AuNP/GCE upon the successive injection of DA in 0.1 mol·L^{-1} PBS (pH 7.0) with the applied potential of 0.2 V. The calibration plot for this DA sensor is shown in Fig. 4B. As illustrated in Fig. 4B, the amperometric response current of DA at GO-MWCNT/MnO$_2$/AuNP/GCE between the concentrations of DA in the range from 5.0×10^{-7} to 2.5×10^{-3} mol·L^{-1} show a good linear relationship with r of 0.9986. This linear fitting equation as follows: I (µA) = 16.49 C (mM) + 0.74. The sensitivity and detection limit of this DA sensor was calculated as 233.4 µA mM^{-1} cm^{-2} and 0.17 µmol·L^{-1} (SNR = 3), respectively.

Comparisons of the electrocatalytic properties with other DA electrochemical sensors are shown in Table 1. As illustrated in Table 1, our sensor showed a wider linear range and a lower

detection limit. It may be attributed to the good electrocatalytic performance of GO-MWCNT/MnO$_2$/AuNP nanocomposites towards the oxidation of DA. Meanwhile, the results of this electrochemical method were also compared with the other reported methods for the detection of DA. These results are listed in Table S1 (ESM). It can be concluded that the electrochemical method can get a lower detection limit and wider linear range.

Reproducibility and stability study

The reproducibility of the GO-MWCNT/MnO$_2$/AuNP/GCE was studied by the chronoamperometry with the applied potential of 0.2 V. The different amperometric response currents to 0.5 mM DA were obtained by five GO-MWCNT/MnO$_2$/ AuNP/GCEs. The relative standard deviation (RSD) of these data was about 3.8 %, suggesting a good reproducibility of the GO-MWCNT/MnO$_2$/AuNP/GCE. The stability of GO-MWCNT/MnO$_2$/AuNP/GCE was also investigated. Three GO-MWCNT/MnO$_2$/AuNP/GCEs were used to detect 0.5 mM DA, and the amperometric response currents were recorded. Amperometric responses remained more than 90 % of its initial value after 25 days, indicating a good stability of the GO-MWCNT/MnO$_2$/AuNP/GCE.

Fig. 4 a Amperometric response obtained by the GO-MWCNT/ MnO$_2$/AuNP/GCE upon the successive injection of DA in 0.1 mol·L^{-1} PBS (pH 7.0) with the applied potential of 0.2 V; **b** Calibration plot of this DA sensor versus its concentration
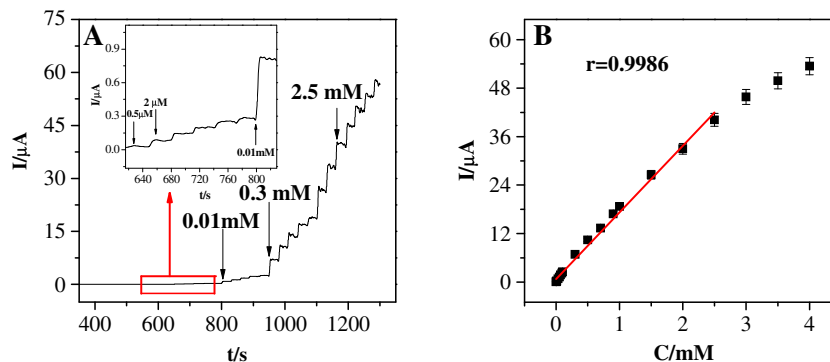
Table 1 Comparison of the electrocatalytic properties with other DA electrochemical sensors for the determination of DA

Sensors	Linear range (μM)	Sensitivity	Detection limit (μM)	References
rGO[a]/Pd/GCE	1–150	2.62 μA μM^{-1} cm^{-2}	0.233	[6]
(GNS/PEI/AuNP/GCE)[b]	2–48	2.64 μA μM^{-1} cm^{-2}	0.2	[21]
tyrosinase-modified ABDD[c] electrode	5–120	68.6 μA mM^{-1} cm^{-2}	1.3	[30]
rGO/TiO$_2$/GCE	2–60	0.622 μA μM^{-1}	6	[31]
nano-ZnO/GCE	0.11–180	–	0.32	[32]
rGO–MWCNT–PTA[d]/GCE	0.5–20	1.56 μA μM^{-1}	1.14	[33]
GO-MWCNT/MnO$_2$/AuNP/GCE	0.5–2500	233.4 μA mM^{-1} cm^{-2}	0.17	This study

− not provided

[a] reduced graphene oxide

[b] graphene nanosheets/polyethyleneimine/gold nanoparticle composite

[c] boron-doped diamond

[d] phospotungstic acid

Selectivity study

The selectivity of the GO-MWCNT/MnO$_2$/AuNP/GCE for other common electroactive species was carefully studied. In this study, the hydrogen peroxide (H$_2$O$_2$), uric acid (UA), glucose, glycine and ascorbic acid (AA) were used as electroactive species. Figure 5 shows the amperometric responses of the GO-MWCNT/MnO$_2$/AuNP/GCE on addition of DA, H$_2$O$_2$, UA, glycine, AA, DA (0.4 mM, respectively) and glucose (4.0 mM) in 0.1 mol·L^{-1} PBS (pH 7.0) with the applied potential of 0.2 V. As shown in Fig. 5, after the addition of 0.4 mM DA, the obvious amperometric responses were quickly displayed. After the addition of 0.4 mM H$_2$O$_2$, the response current only increased by 4.3 %. Moreover, no notable amperometric responses were observed when 0.4 mM each of UA, glycine, AA and 10-fold glucose (4.0 mM) were introduced into the 0.1 mol·L^{-1} PBS (pH 7.0), indicating a

good selectivity of the GO-MWCNT/MnO$_2$/AuNP/GCE. The optimized oxidation potential of DA at the GO-MWCNT/MnO$_2$/AuNP/GCE was 0.2 V and different from other biogenic amines. Thus, at the best potential, the selectivity of this DA sensor is better than that for amperometric detection of other biogenic amines.

Real sample analysis

The real sample analysis ability of the GO-MWCNT/MnO$_2$/AuNP/GCE was also evaluated by the standard addition method. The human serum samples were used as real samples. The results are listed in Table S2 (ESM). The recoveries of this experiment from 98.3 to 101.3 % and the RSD within 3.12 % were calculated. Therefore, the GO-MWCNT/MnO$_2$/Au/GCE has an ability to detect a serum sample.
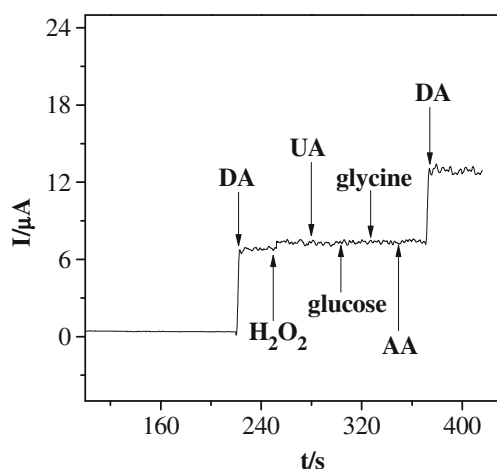
Conclusions

In summary, the AuNPs were successfully self-assembled onto the multilayer films of GO-MWCNT/MnO$_2$ composites with PDDA as a coupling agent. The AuNPs deposited onto the surface of GO-MWCNT/MnO$_2$ composites did not aggregate. Moreover, a high-performance electrochemical sensor of DA based on a GCE modified with the obtained GO-MWCNT/MnO$_2$/AuNP nanocomposites was developed. The DA sensor showed excellent electrocatalytic properties, including a wide linear range, a low detection limit and a high sensitivity. This study potentially constructed an electrochemical sensing platform for the practical detection of DA. Additionally, it is very necessary to conduct further research to improve the stability and durability of the modified electrode in our future work.

Fig. 5 Amperometric responses obtained by the GO-MWCNT/MnO$_2$/AuNP/GCE on successive addition of DA, H$_2$O$_2$, UA, glycine, AA, DA (0.4 mM, respectively) and glucose (4.0 mM) in 0.1 mol·L^{-1} PBS (pH 7.0) with an applied potential of 0.2 V

Compliance with Ethical Standards The author(s) declare that they have no competing interests.

References

1. Lin YH, Chen CE, Wang CY, Pu F, Ren JS, Qu XG (2011) Silver nanoprobe for sensitive and selective colorimetric detection of dopamine via robust Ag-catechol interaction. Chem Commun 47: 1181–1183

2. Ji X, Palui G, Avellini T, Na HB, Yi C, Knappenberger KL Jr, Mattoussi H (2012) On the pH-dependent quenching of quantum dot photoluminescence by redox active dopamine. J Am Chem Soc 134:6006–6017

3. Kumar U, Patel SC (2007) Immunohistochemical localization of dopamine receptor subtypes (D1R-D5R) in Alzheimer's disease brain. Brain Res 1131:187–196

4. El-Beqqali A, Kussak A, Abdel-Rehim M (2007) Determination of dopamine and serotonin in human urine samples utilizing microextraction online with liquid chromatography/electrospray tandem mass spectrometry. J Sep Sci 30:421–424

5. Vikraman AE, Jose AR, Jacob M, Kumar KG (2015) Thioglycolic acid capped CdS quantum dots as a fluorescent probe for the nanomolar determination of dopamine. Anal Methods 7:6791–6798

6. Palanisamy S, Ku S, Chen SM (2013) Dopamine sensor based on a glassy carbon electrode modified with a reduced graphene oxide and palladium nanoparticles composite. Microchim Acta 180: 1037–1042

7. Wu LN, Tan YL, Wang L, Sun SN, Qu ZY, Zhang JM, Fan YJ (2015) Dopamine sensor based on a hybrid material composed of cuprous oxide hollow microspheres and carbon black. Microchim Acta 182:1361–1369

8. Rafati AA, Afraz A, Hajian A, Assari P (2014) Simultaneous determination of ascorbic acid, dopamine, and uric acid using a carbon paste electrode modified with multiwalled carbon nanotubes, ionic liquid, and palladium nanoparticles. Microchim Acta 181: 1999–2008

9. Sanghavi BJ, Wolfbeis OS, Hirsch T, Swami NS (2015) Nanomaterial-based electrochemical sensing of neurological drugs and neurotransmitters. Microchim Acta 182:1–41

10. Tung VC, Huang JH, Tevis I, Kim F, Kim J, Chu CW, Stupp SI, Huang J (2011) Surfactant-free water-processable photoconductive all-carbon composite. J Am Chem Soc 133:4940–4947

11. Zhu Y, Murali S, Cai W, Li X, Suk JW, Potts JR, Ruoff RS (2010) Graphene and graphene oxide: synthesis, properties, and applications. Adv Mater 22:3906–3924

12. Lin KC, Lin YC, Chen SM (2013) A highly sensitive nonenzymatic glucose sensor based on multi-walled carbon nanotubes decorated with nickel and copper nanoparticles. Electrochim Acta 96:164–172

13. Gao W, Tjiu WW, Wei J, Liu T (2014) Highly sensitive nonenzymatic glucose and H_2O_2 sensor based on Ni(OH)$_2$/electroreduced graphene oxide-multiwalled carbon nanotube film modified glass carbon electrode. Talanta 120:484–490

14. Shen JF, Hu YZ, Shi M, Li N, Ma HW, Ye MX (2010) One step synthesis of graphene oxide-magnetic nanoparticle composite. J Phys Chem C 114:1498–1503

15. Hu FX, Chen SH, Wang CY, Yuan R, Yuan DH, Wang C (2012) Study on the application of reduced graphene oxide and multiwall carbon nanotubes hybrid materials for simultaneous determination of catechol, hydroquinone, p-cresol and nitrite. Anal Chim Acta 724:40–46

16. Yang YJ, Li W (2014) CTAB functionalized graphene oxide/multiwalled carbon nanotube composite modified electrode for the simultaneous determination of ascorbic acid, dopamine, uric acid and nitrite. Biosens Bioelectron 56:300–306

17. Lee JH, Hong HG (2015) Nonenzymatic electrochemical sensing of hydrogen peroxide based on a polyaniline-MnO$_2$ nanofiber-modified glassy carbon electrode. J Appl Electrochem 45:1153–1162

18. Wang XJ, Luo CN, Li LL, Duan HM (2015) Highly selective and sensitive electrochemical sensor for l-cysteine detection based on graphene oxide/multiwalled carbon nanotube/manganese dioxide/gold nanoparticles composite. J Electroanal Chem 757:100–106

19. Gan T, Sun JR, Wu WZ, Huang KJ, Zhu JJ (2013) Electrochemical determination of dopamine using a mesoporous MnO$_2$/Polypyrrole-modified electrode. Nanosci Nanotech Let 5:673–676

20. Wang J (2012) Electrochemical biosensing based on noble metal nanoparticles. Microchim Acta 177:245–270

21. Ponnusamy VK, Mani V, Chen SM, Huang WT, Jen JF (2014) Rapid microwave assisted synthesis of graphene nanosheets/polyethyleneimine/gold nanoparticle composite and its application to the selective electrochemical determination of dopamine. Talanta 120:148–157

22. Yusoff N, Pandikumar A, Ramaraj R, Ngee LH, Huang NM (2015) Gold nanoparticle based optical and electrochemical sensing of dopamine. Microchim Acta 182:2091–2114

23. Hou SH, Ou ZM, Chen Q, Wu BY (2012) Amperometric acetylcholine biosensor based on self-assembly of gold nanoparticles and acetylcholinesterase on the sol-gel/multi-walled carbon nanotubes/choline oxidase composite-modified platinum electrode. Biosens Bioelectron 33:44–49

24. Luo GQ, Jiang XJ, Li MJ, Shen Q, Zhang LM, Yu HG (2013) Facile fabrication and enhanced photocatalytic performance of ag/agcl/rgo heterostructure photocatalyst. ACS Appl Mater Inter 5:2161–2168

25. Frens G (1972) Controlled nucleation for regulation of particle-size in monodisperse gold suspensions. Nature 241:20–22

26. Aboutalebi SH, Chidembo AT, Salari M, Konstantinov K, Wexler D, Liu HK, Dou SX (2011) Comparison of GO, GO/MWCNT composites and MWCNTs as potential electrode materials for supercapacitors. Energ Environ Sci 4:1855–1865

27. Fu X, Bei F, Wang X, O'Brien S, Lombardi JR (2010) Excitation profile of surface-enhanced Raman scattering in graphene-metal nanoparticle based derivatives. Nanoscale 2:1461–1466

28. Chen D, Wang G, Lua W, Zhang H, Li JH (2007) Photoelectrochemical study of organic-inorganic hybrid thin films via electrostatic layer-by-layer assembly. Electrochem Commun 9: 2151–2156

29. Bath BD, Michael DJ, Trafton BJ, Joseph JD, Runnels PL, Wightman RM (2000) Subsecond adsorption and desorption of dopamine at carbon-fiber microelectrodes. Anal Chem 72:5994–6002

30. Zhou YL, Tian RH, Zhi JF (2007) Amperometric biosensor based on tyrosinase immobilized on a boron-doped diamond electrode. Biosens Bioelectron 22:822–828

31. How GTS, Pandikumar A, Ming HN, Ngee LH (2014) Highly exposed {001} facets of titanium dioxide modified with reduced graphene oxide for dopamine sensing. Sci Rep 4:5044

32. Xia C, Wang N, Wang L, Guo L (2010) Synthesis of nanochain-assembled ZnO flowers and their application to dopamine sensing. Sensor Actuat B-Chem 147:629–634

33. Ling YY, Huang QA, Zhu MS, Feng DX, Li XZ, Wei Y (2013) A facile one-step electrochemical fabrication of reduced graphene oxide-mutilwall carbon nanotubes–phospotungstic acid composite for dopamine sensing. J Electroanal Chem 693:9–15